Comparative energetic assessment of methanol production from CO_2: Chemical versus electrochemical process

Haitham Al-Kalbani, Jin Xuan, Susana Garc á, Huizhi Wang*

School of Engineering and Physical Sciences, Heriot-Watt University, Edinburgh, United Kingdom, EH14 4AS

*Corresponding author. Tel.: +44 0 131 451 8354; fax: +44 0 131 451 3129.

Email address: h.wang@hw.ac.uk (H.Wang)

Abstract

Emerging emission-to-liquid (eTL) technologies that produce liquid fuels from CO_2 are a possible solution for both the global issues of greenhouse gas emissions and fossil fuel depletion. Among those technologies, CO_2 hydrogenation and high-temperature CO_2 electrolysis are two promising options suitable for large-scale applications. In this study, two CO_2-to-methanol conversion processes, i.e., production of methanol by CO_2 hydrogenation and production of methanol based on high-temperature CO_2 electrolysis, are simulated using Aspen HYSYS. With Aspen Energy Analyzer, heat exchanger networks are optimized and minimal energy requirements are determined for the two different processes. The two processes are compared in terms of energy requirement and climate impact. It is found that the methanol production based on CO_2 electrolysis has an energy efficiency of 41%, almost double that of the CO_2 hydrogenation process provided that the required hydrogen is sourced from water electrolysis. The hydrogenation process produces more CO_2 when fossil fuel energy sources are used, but can result in more negative CO_2 emissions with renewable energies. The study reveals that both of the eTL processes can outperform the conventional fossil-fuel-based methanol production process in climate impacts as long as the renewable energy sources are implemented.

Keywords: Carbon dioxide recycling; Methanol; Carbon dioxide hydrogenation; High temperature electrolysis; Pinch analysis

1. Introduction

Carbon dioxide (CO_2) is the main greenhouse gas responsible for the climate change all over the world. How to reduce CO_2 emissions is a main agenda in many countries and has received substantial research attention [1-4]. Emission-to-liquid (eTL) conversion is a promising technology to reduce carbon emissions as it directly consumes CO_2 as a reactant and at the same time produces useful liquid fuels compatible to the current energy infrastructure. Among various possible fuel products, methanol is of particular interest as it is an energy carrier that can be used for gasoline blending or direct methanol fuel cells [5-6]. In addition, it is a chemical feedstock for production of many valuable chemicals such as formaldehyde, acetic acid, methyl methacrylate, dimethyl terephthalate, methylamines, chloromethanes, dimethyl carbonate and methyl tertiary butyl ether [7]. It can also be transformed to ethylene and propylene via methanol-to-olefin (MTO) processes [8]. The current annual consumption of methanol is over 60 million metric tons globally, and it keeps growing [9]. However, almost all methanol produced worldwide is synthesized from fossil-fuel-based syngas, which is neither sustainable nor environmentally-friendly [10-11]. The eTL process kills two birds with one stone by enabling sustainable methanol production, and at the same time, reducing atmospheric CO_2 levels.

So far, the synthesis of methanol from CO_2 has been successfully demonstrated using photocatalytic, electrochemical and chemical (catalytic hydrogenation) methods. Though photocatalytic reduction of CO_2 is an attractive option as it allows for a direct use of solar energy, it is limited to lab-scale studies due to the sluggish kinetics and extremely low efficiency [12-14]. In contrast, CO_2 electrolysis in a high temperature solid oxide electrolytic cell (SOEC) and catalytic CO_2 hydrogenation show great potential for large-scale applications and thereby large-scale CO_2 consumption [15-16]. After decades of efforts in exploiting effective catalyst materials and developing advanced reactors, catalytic CO_2

hydrogenation has become technically competitive with the industrial production of methanol from syngas [17-20]. Different pilot plants have been constructed in Japan and Iceland to produce methanol from hydrogenation of CO_2 with renewable H_2 [20]. A recent techno-economic study revealed that the use of CO_2 hydrogenation for methanol production can be economically viable as long as the costs of raw materials, i.e., H_2 and captured CO_2, can be reduced [21]. On the other hand, R&D activity for high-temperature CO_2 electrolysis is accelerating [16]. One attractive feature of the electrochemical conversion of CO_2 is that it provides a possible solution to the storage of intermittent renewable electricity [22]. To date, substantial studies have been reported in various technical aspects of CO_2 electrolysis, including new electrocatalyts, reaction mechanisms, catalyst degradation, cell design and system design [23-28]. Despite significant technical advances in both of the technologies, there has been a lack of systematic comparison of different CO_2-to-methanol processes. Once technologically mature, there is an ambiguity in selection between the processes.

In this study, the two CO_2-to-methanol conversion processes, i.e., production of methanol by CO_2 hydrogenation and production of methanol based on high-temperature CO_2 electrolysis, are simulated and analysed using Aspen HYSYS. Using Aspen Energy Analyzer (AEA), heat exchanger networks (HEN) are optimized for both the processes, and their associated minimal energy requirements are determined. The two processes are finally compared in terms of energy requirement and climate impact. The results in this study will shed light on the further development of various eTL processes.

2. Methods

2.1. Process description

2.1.1. Methanol production from CO_2 hydrogenation

The process of methanol production from CO_2 hydrogenation is illustrated in Fig. 1(a), which consists of four main steps, i.e., CO_2 capture, H_2 production, methanol synthesis and methanol purification. The input streams to this process are flue gas (2 bar, 313 K) and water (1.01 bar, 298 K). In a global context, fossil-fuel-based power plants which are responsible for ~57% of the total CO_2 emissions are reported as the largest CO_2 emitter [29], and thus they are considered as the source of CO_2 in this study. Carbon capture process is firstly employed to separate CO_2 from flue gases from a thermal power plant. Substantial efforts have been made, particularly in recent years, to develop effective carbon capture technologies as a potentially immediate way to reduce the carbon intensity. The existing technologies for CO_2 separation and capture for power plants can be divided into three different categories, namely, post-combustion processes for a traditional coal-fired power plant, pre-combustion processes for gasification or reforming and oxy-fuel processes [30]. Post-combustion capture by liquid absorption using monoethanolamine (MEA) has been identified to be the most promising technology to date in terms of effectiveness and cost [31-33]. Water is here used as a source of H_2. With an electrolysis system, water is decomposed into stoichiometric amounts of H_2 and O_2. Compared to other available hydrogen production methods, water electrolysis has advantages of wide availability, flexibility and high purity of products. Though the high cost associated with the use of precious-metal catalysts remains an issue for the widespread application of this technology, it provides the best way for large-scale storage of intermittent renewable electricity. The produced H_2, together with the captured CO_2, are sent to a methanol synthesis unit for methanol production, which is normally operated in a temperature range of 493~543 K [13]. Following the methanol synthesis step, methanol purification is applied where a series of distillation columns are used to remove impurities from the methanol product. Fig. 1(b) shows our model layout.

2.1.2. Methanol production based on a high-temperature SOEC system

Fig. 2(a) schematically shows the process of methanol production based on a high-temperature SOEC system. Four steps are involved in this process, which are CO_2 capture, high-temperature electrolysis, methanol synthesis and methanol purification. Similar to the CO_2 hydrogenation process, water (1.01 bar, 298 K) and flue gas (2 bar, 313 K) are the input streams to the system. With a carbon capture unit, CO_2 is firstly captured from flue gases of a thermal power plant. The captured CO_2 is then sent to an SOEC system for syngas production together with water after being heated up to 1073 K (i.e., the operating temperature of the SOEC [26]). The resultant gas consisting of CO, CO_2 and H_2O is then passed to a methanol synthesis reactor for methanol generation. Methanol purification is finally performed to ensure the purity of the produced methanol. The corresponding Aspen HYSYS model is shown in Fig. 2(b).

2.2. Process simulation

2.2.1. CO_2 capture unit

Post-combustion capture by liquid absorption using MEA is adopted in the present study. The built-in MEA absorber and generator in Aspen HYSYS is directly used for the simulation. Typical thermal power plant flue gas consisting of, by molarity, 71.4% N_2, 14.6% CO_2, 11.2% water vapour and 2.8% O_2 [34] is fed into the unit for treatment. After leaving the power plant, the flue gas is supplied at 313 K and 2 bar into the bottom of the absorber column where it flows upwards. It flows counter-currently to the MEA which is introduced from the top of the column (called lean amine) and the treated gas is drawn from the top of the tower. The MEA absorbs the CO_2 in the flue gas and then leaves from the bottom of the column (rich amine). The rich amine is regenerated in a stripping column. The heat required by the regeneration process can be a main contributor to the total energy consumption.

Typical energy requirement for the capture of 1 kg of CO_2 is 3~5 MJ according to the literatures [35-36]. The values of the MEA concentration and MEA loading are adjusted to ensure the power consumption fall within this typical range. The CO_2 from the regeneration column is compressed to 67.4 bar, which equals to the pressure of the methanol synthesis reactor. To avoid excessive temperature increase, the compression takes place in four stages, and coolers are added between the stages. The operating conditions of the CO_2 capture unit are summarized in Table 1.

2.2.2. Water electrolysis unit

H_2 necessary for CO_2 hydrogenation is produced from a water electrolysis system. Alkaline water electrolysers are considered in the study as they are a quite mature technology which can offer reasonable efficiency at relatively low costs compared to other emerging water electrolysis technologies [37-39]. The electrolysis system contains a number of alkaline electrolytic cells stacked together to achieve a required gas production capacity. Each single cell consists of an anode and a cathode operating in an aqueous electrolyte solution of potassium hydroxide or sodium hydroxide. A direct current is applied to the cell when operation. The protons in water are reduced at the cathode to form H_2 gas by combining the electrons coming from the external circuit.

Cathode: $2H^+ + 2e^- \rightarrow H_2$ (1)

At the anode, the below oxidation reaction occurs, generating O_2 gas and giving electrons to the cathode to complete the circuit.

Anode: $2OH^- \rightarrow 0.5O_2 + H_2O + 2e^-$ (2)

The overall reaction of the water electrolysis is therefore written as

$$H_2O \rightarrow H_2 + 0.5\ O_2 \quad (3)$$

The generated O_2 from this step is assumed to be vented to the atmosphere. To produce 1 m^3 of H_2 under STP conditions, a state-of-the-art alkaline water electrolysis system requires an energy input of 4~5 kWh_{el} [36]. The system provides H_2 at 30 bar and 298 K, which is then compressed in one stage to the required reactor pressure of 67.4 bar.

2.2.3. Methanol synthesis and purification unit

Two types of methanol synthesis reactors are generally used in industrial production processes, i.e., a quench reactor consisting of a series of adiabatic beds where fresh syngas is introduced among the beds, and a Lurgi-type shell-tube reactor where the tubes are filled with catalysts and the heat released from the reactions is removed by circulating water on the shell side to produce medium pressure steam. In our model, the isothermal operation of the latter reactor is selected. The reactor is modelled as a plug flow reactor using Aspen HYSYS. The temperature in the plug flow reactor rises steadily along the flow direction and the heat generated by reactions is simulated as a direct heat source. The temperature profile within the reactor is determined by the specified inlet and outlet temperatures. Using this approach, the reactor sensitivity to coolant can be eliminated. The inlet stream is fed at 538 K, and gases are cooled down to 313 K after leaving the reactor so that methanol can be separated from the effluent by a two-phase separator. The remaining unreacted gases are compressed and looped back to the inlet of the reactor. The recycle stream is partly purged with a purge gas to avoid the formation of an inert atmosphere in the loop. Herein, industry standard of recycle ratio (i.e., the ratio of recycle gas to fed syngas) between 3:1 and 7:1 is adopted, and the purge gas is set as 1.0 mol % of the recycle stream. The recycle function in Aspen HYSYS is tuned in terms of sensitivity by setting sensitivity to flowrate as 1, composition as 0.1 and enthalpy as 0.1 to ensure the accuracy by avoiding any major change on the parameters. The catalysts and reactor dimensions in the study follow those reported by Chen et al. [40], and they are listed

in Table 2. The pressure drop across the reactor is fixed to be 3.3 bar. By adjusting the size of the reactor, a daily methanol production of 1500 ton is achieved, which represents typical values of a medium-scale plant. It is noted that the stoichiometric ratio of syngas, λ, defined in Eq. (4) has an optimal value of 2 when used for methanol synthesis.

$$\lambda = (N_{H2} - N_{CO2}) / (N_{CO} + N_{CO2}) \quad (4)$$

where N denotes the number of moles of each species. For CO_2 hydrogenation, the amounts of the feed stocks (flue gas and H_2O) are adjusted to match the required $\lambda = 2$, whereas for the case of high temperature co-electrolysis, the amounts of water and flue gas supplied to the cell are adjusted to obtain a λ value of 2. In the reactor, two methanol production reactions (Eqs.(5) and (6)) and a reverse water gas shift (RWGS) reaction (Eq. (7)) generally take place and thus they are taken into account [36]

$$CO_{2\,(g)} + 3H_{2(g)} \leftrightarrow CH_3OH_{(l)} + H_2O_{(g)} \quad \Delta H = -87 \text{ kJ mol}^{-1} \text{ (298 K)} \quad (5)$$

$$CO_{(g)} + 2H_{2(g)} \leftrightarrow CH_3OH_{(l)} \quad \Delta H = -128 \text{ kJ mol}^{-1} \text{ (298 K)} \quad (6)$$

$$CO_{(g)} + H_2O_{(g)} \leftrightarrow CO_{2(g)} + H_{2(g)} \quad \Delta H = +41 \text{ kJ mol}^{-1} \text{ (298 K)} \quad (7)$$

The kinetics of the above reactions have been modelled by Bussche and Froment [41] as follows

$$r_{CH_3OH} = \frac{k_1 p_{CO_2} p_{H_2} \left(1 - \frac{1}{K_{eq1}} \frac{p_{H_2O} p_{CH_3OH}}{p_{H_2}^3 p_{CO_2}}\right)}{\left(1 + k_2 \frac{p_{H_2O}}{p_{H_2}} + k_3 p_{H_2}^{0.5} + k_4 p_{H_2O}\right)^3} \left[\frac{mol}{kg_{cat} s}\right] \quad (8)$$

$$r_{RWGS} = \frac{k_5 p_{CO_2} \left(1 - K_{eq2} \frac{p_{H_2O} p_{CO}}{p_{H_2} p_{CO_2}}\right)}{\left(1 + k_2 \frac{p_{H_2O}}{p_{H_2}} + k_3 p_{H_2}^{0.5} + k_4 p_{H_2O}\right)} \left[\frac{mol}{kg_{cat} s}\right] \quad (9)$$

$$k_i = A_i \exp\left(\frac{B_i}{RT}\right) \tag{10}$$

$$\log_{10} K_{eq1} = \frac{3066}{T} - 10.592 \tag{11}$$

$$\log_{10} \frac{1}{K_{eq2}} = 2.029 - \frac{2073}{T} \tag{12}$$

where r is reaction rate, A, B and $k_{1\text{-}5}$ are kinetic model constants, p is partial pressure, K_{eq} is equilibrium constant, R is molar gas constant (8.314 J mol^{-1} K^{-1}) and T is temperature. The model by Bussche and Froment has already been widely adopted in previous studies on process simulation [36, 42], and thus is used here. Eqs. (8)-(12) are modified following the method detailed elsewhere [36] before implementing in Aspen HYSYS. Table 3 shows the kinetic parameters.

The methanol purification is modelled in two steps which are a flash drum operating at 2 bar and a distillation column. Most of gases are released from the flash drum and then they enter a distillation column with 32 stages. The purification unit is able to reach a methanol purity of 99.5 wt.%. The reflux ratio is adjusted to determine the required cooling duty.

2.2.4. SOEC unit

There are three reactions occurring in an SOEC for water/CO_2 co-electrolysis, i.e., water electrolysis, CO_2 electrolysis and RWGS [43-44]. During the operation, water and CO_2 are reduced to H_2 and CO at the cathode via reactions (13) and (14), respectively.

Cathode:

$$H_2O + 2e^- \rightarrow H_2 + O^{2-} \tag{13}$$

$$CO_2 + 2e^- \rightarrow CO + O^{2-} \tag{14}$$

The produced oxygen ions (O^{2-}) transport through a solid oxide electrolyte (e.g., yttrium-stabilised zirconia, YSZ) to the anode, where they lose electrons to form O_2

Anode: $2O^{2-} \rightarrow O_2 + 4e^-$ (15)

The overall reaction is written as

Overall: $CO_2 + H_2O \rightarrow CO + H_2 + O_2$ (16)

Apart from the above electrochemical reactions, the RWGS reaction described in Eq. (7) also takes place in the cathode due to the presence of Ni catalysts in the electrode.

The SOEC unit modelled here is composed of a number of SOECs in stacks, and it is assumed to be operated isothermally at 1073 K. Water and CO_2 are supplied as the input streams together with a recycle stream exiting from the unit. The recycle stream contains H_2 and CO, which creates a reducing environment at the cathode to avoid undesired oxidation reactions [45]. The reactants mixture is heated up to the cell temperature (i.e., 1073 K), and passes an equilibrium reactor where a chemical equilibrium among the species including CO, CO_2, H_2O and H_2 is attained. The resultant equilibrium mixture is supplied as a cathode reactant to the SOEC unit for syngas generation. For the oxygen evolving anode, no sweep gas is applied in this study in view of a higher thermal efficiency under the non-swept condition [45].

As electrolysers are not a standard HYSYS component, a custom model of electrolysers developed in the literatures [26, 46] is employed for the modelling of the SOEC unit. The initial values of the amounts of CO_2 and water are firstly set by assuming a daily methanol production of 2000 ton from reaction (5). With these initial values, the amount of O_2 generated by reaction Eq. (16) can be calculated using HYSYS based on 100% conversion of CO_2 and water. Using Faraday's law, the number of cells in the SOEC unit can be estimated from the calculated O_2 amount. However, a steam utilisation above 90% is unrealistic due to localised steam starvation. Maximum utilization efficiencies were recently reported to be 77 % and 76% respectively for the steam and CO_2 [47]. Thus, it is reasonable to assume that both the steam and CO_2 in this study have utilization efficiency of 70%. Once the number of

cells is calculated, it is used as an input parameter to the model. The number of cells is then altered until the prescribed conversion rate of 70% is achieved. The electrical power required by the SOEC unit is written as

$$W = V_{\text{op}} I = V_{\text{op}} \times i \times A_{cell} \tag{17}$$

where V_{op} is the average cell voltage during operation, I is the total current, i is the current density and A_{cell} is the total active area in the SOEC stack. The value of V_{op} can be expressed as a function of the current density [26, 46]

$$V_{OP} = \overline{V_N} + i \cdot ASR \tag{18}$$

In the above equation, $\overline{V_N}$ and ASR respectively denote the mean Nernst potential of the cell and the mean area specific resistance of the SOEC stack, which depend on the species concentrations and temperature in the stack [26]

$$\overline{V_N} = -0.5\left(\frac{RT_R}{4F} \ln p_{O_2,R} + \frac{RT_P}{4F} \ln p_{O_2,P} \right) \tag{19}$$

$$ASR = ASR^0 - 0.462 + 3.973 \times 10^{-5} \exp\left(\frac{10300}{T} \right) \tag{20}$$

where the subscripts R and P denotes reactant gas and product gas, respectively. ASR^0 in Eq. (20) is the mean area specific resistance of the SOEC stack at 1100 K, and a typical value from solid oxide fuel cell stacks (which share the same hardware with SOEC but operate in a reverse process) is adopted here [45].

The enthalpy change across the SOEC converter and a second shift reactor is reported as the extra heat required for the reaction after subtracting the electrical power of electrolysis. The required heat of reactions includes both the electrical and thermal energies. Table 4 summarizes the parameter inputs for the SOEC model. The present design of SOEC unit allows for a methanol production of 1525 ton per day.

2.2.5. Waste heat recovery unit

The steam generated with the heat removed from the methanol synthesis reactor is passed to a turbo-expander for further electricity production. Fig. 3(a) shows the electricity production process, which is accomplished by a boiler and a pump that increases the pressure of the water fed to the boiler to 40 bar. In addition, energies are also recovered from the combustible emissions, which mainly come from (i) the methanol recycle loop purge gas, (ii) the flash vessel and (iii) the methanol distillation column. As depicted in Fig. 3(b), the emissions from the above three sources are firstly combined together and sent to a conversion reactor where they are combusted. It is assumed that 85 % of the emissions are burnt out. The produced heat is used to generate low-pressure steam, which is then used in a Rankine cycle for electricity generation.

2.3. Heat integration and energy demand

The heat integration is performed using pinch analysis to determine the minimum heating and cooling utilities required by each process. By doing this, heat recovery and utilisation can be maximized through exchanging the heat between cold and hot streams instead of introducing extra heat. The minimum requirement of heating and cooling utilities is calculated from the minimum temperature difference between the hot and cold streams ($\Delta T_{\min}$) by the AEA. As mentioned, the spent utilities can be used to generate electricity through the Rankine cycle. It is noted that the medium pressure steam produced on the shell side of the methanol synthesis reactor is not included here as a utility. For each of the processes, two different scenarios are considered when doing the pinch analysis: (i) an integrated scenario where energy exchange is allowed among all the streams, and (ii) a segregated scenario where each sub-process runs independently and no energy exchanges

between them. The second scenario is modelled because it eliminates the dependence of one sub-process on another and can be advantageous during start-up.

3. Results and discussion

3.1. Heat integration

3.1.1. Methanol production from CO_2 hydrogenation

Figs. 4(a) and (b) respectively show the composite curves and the grand composite curves for the process of methanol production from CO_2 hydrogenation under the integrated scenario. Fig. 4(a) indicates that there is a process to process pinch point at 384 K. According to Fig. 4 (b), the minimum hot and cold utilities required under this scenario are 122.3 MW_{th} and 281.1 MW_{th}, respectively. For the segregated scenario, the sub-processes of carbon capture and methanol production are treated as two independent processes. Figs. 4(c) and (d) respectively plot the composite curves and the grand composite curves for the carbon capture process, and Figs. 4(e) and (f) gives those curves for the methanol production process. By summing up the values of the two independent processes, the total minimum amounts of heating and cooling required by the segregated scenario are 142.1 MW_{th} and 301.1 MW_{th} respectively.

The HEN is optimized for the integrated scenario in Fig. 5(a), which includes 8 process-process heat exchangers (white matches), 11 heat exchangers with cold utilities (blue matches) and 6 heat exchangers with hot utilities (red matches). The total surface area for heat exchange is 4.0×10^4 m^2. With the optimal HEN, the heating and cooling utilities are reduced by 50% and 31%, respectively. In the segregated scenario, the HEN is optimized separately for the carbon capture and methanol production with the results shown in Figs. 5(b) and (c). According to Fig. 5(b), there is only one heat exchanger in the carbon capture process. The remaining heating and cooling requirements are supplied by the utilities

resulting in the use of 5 heat exchangers with cold utilities and 2 heat exchangers with hot utilities. Though three heaters are installed in our original design of the hydrogenation process in Fig. 1(b) to reduce the CO_2 temperature among the stages of compression, these streams (H3, H4 and H5) are not useful for heat exchange due to the low loads and lack of a receiver for those loads. They eventually become a heat sink to the cold utility. The segregated scenario shows a reduction of 42.6% in heating and 26.3% in cooling utilities after optimization, which is achieved by a heat exchange area of 4.2×10^4 m^2.

3.1.2. Methanol production based on a high-temperature SOEC unit

The composite curves and the grand composite curves for the production of methanol based on the high-temperature electrolysis are shown in Fig. 6. Under the integrated scenario, the composite curves in Fig. 6(a) indicate that there are multiple pinch points at 313 K, 376.9 K and 400.8 K, respectively. According to Fig. 6(b), the minimum amounts of heating and cooling utilities under this scenario respectively are 112.5 MW_{th} and 156.5 MW_{th}. For the segregated scenario where the sub-processes of carbon capture, co-electrolysis and methanol production are independent of each other, the composite curves and the grand composite curves are plotted for each different process in Figs. 6(c) - (h). It is seen from the figures that the total amounts of heating and cooling utilities under the segregated scenario are 207.5 MW_{th} and 251.5 MW_{th}, respectively.

Fig. 7(a) shows an optimized HEN for the integrated SOEC-based process. There are 55 heat exchangers between the processes and utilities. With the optimal HEN design, the heating and cooling utilities can be reduced respectively by 67.3% and 59.7% compared with the original design in Fig. 2. For the segregated scenario, the HENs are optimized separately for the processes of carbon capture, high-temperature electrolysis and methanol production, as shown in Figs. 7(b), (c) and (d), respectively. Summing up the heating and cooling utilities

required by the three optimized processes can result in heating and cooling utilities 39.7% and 35.2 % lower than those of the non-optimized process.

3.2. Comparison of energy requirements

The energy requirements of the different CO_2-to-methanol processes are analysed and compared. It is noted that there is no difference between the electricity consumption under integrated and segregated scenarios because the heat integration is only performed to the hot and cold streams. Fig. 8(a) compares the demands of different forms of energy in the hydrogenation process under different scenarios. For both the integrated and segregated scenarios, the demands of electricity are found to be much higher than those of heating and cooling. This is attributed to the high electricity requirement by the water electrolysis. Only slight difference is observed between the two scenarios in heating and cooling requirements. There is only one high-grade stream (i.e., methanol reactor effluent) which supplies heat to a number of cold streams. Due to the large heat requirement of carbon capture and methanol synthesis, the stream can be fully utilised regardless if the case is integrated or not. Fig. 8(b) shows the demands of different types of energy in the SOEC-based process. Compared to the hydrogenation process, the SOEC-based process requires much more heating energy but has lower electricity demand. This is due to the high operating temperature of the co-electrolysis. Under the integrated scenario, the heating and cooling utilities are respectively reduced by 15% and 37% in comparison with those in the segregated scenario.

The overall energy consumption of the two processes is compared in Fig. 8(c). In both the integrated and segregated scenarios, the hydrogenation process requires more energy, which nearly doubles the SOEC-based process. It is found that 93% of the total energy demand for the hydrogenation process is contributed by the water electrolysis. If the heat recovery from the steam is considered, the overall energy requirements of both processes can slightly

decrease. As shown in Fig. 8(d), the energy consumption of the production of 1 ton methanol decreases from 91.0 to 88.7 GJ_{th} if the steam is used as a heating medium for the integrated hydrogenation process, and from 48.2 to 45.4 GJ_{th} for the integrated SOEC-based process. The energy efficiency of different processes, η, defined as the ratio of energy output to energy input, is evaluated using the following equation [45]

$$\eta = \frac{LHV_{MeOH} N_{MeOH}}{\sum_{i,R} Q_{in} + \sum_{i,R} N_{i,R} LHV_{i,R}} \tag{21}$$

where LHV is lower heating value, Q_{in} is the heat input to the system. The energy efficiencies of the hydrogenation and SOEC-based processes are compared in Fig. 8(e). The SOEC-based process doubles the energy efficiency of hydrogenation process no matter how the waste energy is utilized. This reflects the huge percentage of electricity required for water electrolysis which when converted to thermal energy results in higher denominator of Eq. (21).

3.3. Comparison of carbon emissions

Carbon emission is another important aspect when evaluating a production process. The CO_2 equivalent can be evaluated using the following equation [48,49]

$$m_{net} = m_{hysys} + m_{elec} + m_{therm} - m_{pp} \tag{22}$$

where m is mass of CO_2. The subscripts net, hysys, elec, therm and pp respectively are the net CO_2 release, CO_2 release from the HYSYS model, CO_2 release from the electricity, CO_2 release from the thermal energy demand, and CO_2 release from the power plant. Fig. 9 compares the CO_2 equivalents emitted from the two different CO_2-to-methanol processes. The power required to drive the two eTL processes is considered to be sourced from four different energy sources including coal, natural gas, solar PV and onshore wind. According to

the figure, the hydrogenation process results in higher CO_2 emissions when gas combined cycle and coal are used for energy supply. With renewable energy sources such as onshore wind and solar energy, however, the hydrogenation process generates more negative CO_2 emissions. This is due to the fact that both the gas combined cycle and coal-based electricity lead to a high CO_2 release, and the electricity is responsible for over 90% of the total energy consumption of the hydrogenation process. On the other hand, the renewable energies correspond to lower CO_2 emissions, which give more negative net release of CO_2. Compared to the carbon emission of the conventional fossil-fuel-based methanol production which was reported to be 0.79 kg CO_2-eq kg^{-1} CH_3OH [49], the net CO_2 emissions of these eTL processes are lower only if relying on renewable energies. The eTL processes can cause severer carbon emissions than the conventional methanol production process if natural gas or coal are used as energy sources.

4. Conclusions

In this study, two CO_2-to-methanol conversion processes, i.e., production of methanol by CO_2 hydrogenation and production of methanol based on high-temperature CO_2 electrolysis, are simulated using Aspen HYSYS. With the AEA, HENs are optimized and minimal energy requirements are determined for the two different processes. The two processes are compared to each other in terms of energy requirement and climate impact. It is found that the production of methanol based on high-temperature electrolysis leads to a much lower energy demand than the hydrogenation process. The energy efficiency of the electrolysis-based process is 41%, which almost doubles that of the hydrogenation process. The hydrogenation process can produce more CO_2 when fossil fuel energy sources are used, but result in more negative CO_2 emissions with renewable energies. Both of the eTL processes outperform the

conventional fossil-fuel-based methanol production process in reducing net CO_2 generation only if the renewable energy sources are implemented.

Acknowledgment

This research was supported by the Scottish-Hong Kong SFC / RGC Joint Research Scheme (H15009) and the Global Innovation Initiative Grant No. S-ECAGD-13-CA-149 (DT).

Nomenclature

A	kinetic model constant
B	kinetic model constant (J mol^{-1})
A_{cell}	total active area in SOEC stack (m^2)
ASR	mean area specific resistance of SOEC stack (Ω cm^2)
F	Faraday constant (96485 C mol^{-1})
I	total current (A)
i	current density (A m^{-2})
K_{eq}	equilibrium constant
k	kinetic model constant as a function of A and B
LHV	lower heating value (J mol^{-1})
m	mass (kg)
N	number of moles of species (mol)
p	partial pressure (bar)
Q_{in}	heat input to the system (J)
R	molar gas constant (8.314 J mol^{-1} K^{-1})
r	reaction rate (mol kg_{cat}^{-1} s^{-1})
T	temperature (K)

V_N mean Nernst potential (V)

V_{op} average cell voltage during operation (V)

W electrical power required by SOEC (W)

Greek letters

η energy efficiency

λ stoichiometric ratio of syngas

References

[1] Mundaca L, Román R, Cansino JM. Towards a Green Energy Economy? A macroeconomic-climate evaluation of Sweden's CO_2 emissions. Applied Energy. 2015;148:196-209.

[2] Gambhir A, Tse LKC, Tong D, Martinez-Botas R. Reducing China's road transport sector CO_2 emissions to 2050: Technologies, costs and decomposition analysis. Applied Energy, in press, doi:10.1016/j.apenergy.2015.01.018

[3] Anandarajah G, Gambhir A. India's CO_2 emission pathways to 2050: What role can renewables play? Applied Energy. 2014;131:79-86.

[4] Chen Q, Tang Z, Lei Y, Sun Y, Jiang M. Feasibility analysis of nuclear–coal hybrid energy systems from the perspective of low-carbon development. Applied Energy. 2015;158:619-30.

[5] Hu T, Wei Y, Liu S, Zhou L. Improvement of spark-ignition (SI) engine combustion and emission during cold start, fueled with methanol/gasoline blends. Energy & Fuels. 2007;21:171-5.

[6] Zhao X, Yin M, Ma L, Liang L, Liu C, Liao J, et al. Recent advances in catalysts for direct methanol fuel cells. Energy & Environmental Science. 2011;4:2736-53.

[7] Olah GA. Towards oil independence through renewable methanol chemistry. Angewandte Chemie International Edition. 2013;52:104-7.

[8] Van Speybroeck V, De Wispelaere K, Van der Mynsbrugge J, Vandichel M, Hemelsoet K, Waroquier M. First principle chemical kinetics in zeolites: The methanol-to-olefin process as a case study. Chemical Society Reviews. 2014;43:7326-57.

[9] The Methanol Industry, http://www.methanol.org/Methanol-Basics/The-Methanol-Industry.aspx, accessed in August 2015.

[10] Olah GA. Beyond oil and gas: The methanol economy. Angewandte Chemie International Edition. 2005;44:2636-9.

[11] Steinberg M. Production of hydrogen and methanol from natural gas with reduced CO_2 emission. International Journal of Hydrogen Energy. 1998;23:419-25.

[12] Morris AJ, Meyer GJ, Fujita E. Molecular approaches to the photocatalytic reduction of carbon dioxide for solar fuels. Accounts of Chemical Research. 2009;42:1983-94.

[13] Ganesh I. Conversion of carbon dioxide into methanol-a potential liquid fuel: Fundamental challenges and opportunities (a review). Renewable and Sustainable Energy Reviews. 2014;31:221-57.

[14] Cheng Y-H, Nguyen V-H, Chan H-Y, Wu JCS, Wang W-H. Photo-enhanced hydrogenation of CO_2 to mimic photosynthesis by CO co-feed in a novel twin reactor. Applied Energy. 2015;147:318-24.

[15] Quadrelli EA, Centi G, Duplan J-L, Perathoner S. Carbon dioxide recycling: Emerging large-scale technologies with industrial potential. ChemSusChem. 2011;4:1194-215.

[16] Uhm S, Kim YD. Electrochemical conversion of carbon dioxide in a solid oxide electrolysis cell. Current Applied Physics. 2014;14:672-9.

[17] An X, Li J, Zuo Y, Zhang Q, Wang D, Wang J. A Cu/Zn/Al/Zr fibrous catalyst that is an improved CO_2 hydrogenation to methanol catalyst. Catal Lett. 2007;118:264-9.

[18] Weigel J, Koeppel RA, Baiker A, Wokaun A. Surface species in CO and CO_2 hydrogenation over Copper/Zirconia: On the methanol synthesis mechanism. Langmuir. 1996;12:5319-29.

[19] Gallucci F, Paturzo L, Basile A. An experimental study of CO_2 hydrogenation into methanol involving a zeolite membrane reactor. Chemical Engineering and Processing: Process Intensification. 2004;43:1029-36.

[20] Jadhav SG, Vaidya PD, Bhanage BM, Joshi JB. Catalytic carbon dioxide hydrogenation to methanol: A review of recent studies. Chemical Engineering Research and Design. 2014;92:2557-67.

[21] Pérez-Fortes M, Schöneberger JC, Boulamanti A, Tzimas E. Methanol synthesis using captured CO_2 as raw material: Techno-economic and environmental assessment. Applied Energy, in press, doi:10.1016/j.apenergy.2015.07.067.

[22] Grace AN, Choi SY, Vinoba M, Bhagiyalakshmi M, Chu DH, Yoon Y, et al. Electrochemical reduction of carbon dioxide at low overpotential on a polyaniline/Cu_2O nanocomposite based electrode. Applied Energy. 2014;120:85-94.

[23] Graves C, Ebbesen SD, Mogensen M. Co-electrolysis of CO_2 and H_2O in solid oxide cells: Performance and durability. Solid State Ionics. 2011;192:398-403.

[24] Kim-Lohsoontorn P, Bae J. Electrochemical performance of solid oxide electrolysis cell electrodes under high-temperature coelectrolysis of steam and carbon dioxide. Journal of Power Sources. 2011;196:7161-8.

[25] Ni M. 2D thermal modeling of a solid oxide electrolyzer cell (SOEC) for syngas production by H_2O/CO_2 co-electrolysis. International Journal of Hydrogen Energy. 2012;37:6389-99.

[26] Fu Q, Mabilat C, Zahid M, Brisse A, Gautier L. Syngas production via high-temperature steam/CO_2 co-electrolysis: an economic assessment. Energy & Environmental Science. 2010;3:1382-97.

[27] Ni M. Modeling of a solid oxide electrolysis cell for carbon dioxide electrolysis. Chemical Engineering Journal. 2010;164:246-54.

[28] Stempien JP, Ni M, Sun Q, Chan SH. Thermodynamic analysis of combined Solid Oxide Electrolyzer and Fischer–Tropsch processes. Energy. 2015;81:682-90.

[29] United States Environmental Protection Agency, Global Greenhouse Gas Emissions Data, http://www.epa.gov/climatechange/ghgemissions/global.html

[30] Cuéllar-Franca RM, Azapagic A. Carbon capture, storage and utilisation technologies: A critical analysis and comparison of their life cycle environmental impacts. Journal of CO_2 Utilization. 2015;9:82-102.

[31] Wang M, Lawal A, Stephenson P, Sidders J, Ramshaw C. Post-combustion CO_2 capture with chemical absorption: A state-of-the-art review. Chemical Engineering Research and Design. 2011;89:1609-24.

[32] Sanna A, Ramli I, Mercedes Maroto-Valer M. Development of sodium/lithium/fly ash sorbents for high temperature post-combustion CO_2 capture. Applied Energy. 2015;156:197-206.

[33] Li B-H, Zhang N, Smith R. Simulation and analysis of CO_2 capture process with aqueous monoethanolamine solution. Applied Energy, in press, doi:10.1016/j.apenergy.2015.07.010

[34] Singh D, Croiset E, Douglas PL, Douglas MA. Techno-economic study of CO_2 capture from an existing coal-fired power plant: MEA scrubbing vs. O_2/CO_2 recycle combustion. Energy Conversion and Management. 2003;44:3073-91.

[35] ErikØi L. Comparison of Aspen HYSYS and Aspen Plus simulation of CO_2 absorption into MEA from atmospheric gas. Energy Procedia. 2012;23:360-9.

[36] Van-Dal ÉS, Bouallou C. Design and simulation of a methanol production plant from CO_2 hydrogenation. Journal of Cleaner Production. 2013;57:38-45.

[37] Holladay JD, Hu J, King DL, Wang Y. An overview of hydrogen production technologies. Catalysis Today. 2009;139:244-60.

[38] Zeng K, Zhang D. Recent progress in alkaline water electrolysis for hydrogen production and applications. Progress in Energy and Combustion Science. 2010;36:307-26.

[39] Rashid MM, Al Mesfer MK, Naseem H, Danish M. Hydrogen production by water electrolysis: A review of alkaline water electrolysis, PEM water electrolysis and high temperature water electrolysis. International Journal of Engineering and Advanced Technology. 2015;4:80-93.

[40] Chen L, Jiang Q, Song Z, Posarac D. Optimization of methanol yield from a Lurgi reactor. Chemical Engineering & Technology. 2011;34:817-22.

[41] Bussche KMV, Froment GF. A steady-state kinetic model for methanol synthesis and the water gas shift reaction on a commercial $Cu/ZnO/Al_2O_3$ catalyst. Journal of Catalysis. 1996;161:1-10.

[42] Van-Dal ÉS, Bouallou C. CO_2 abatement through a methanol production process. Chemical Engineering Transactions. 2012;29:463-8.

[43] Ni M. An electrochemical model for syngas production by co-electrolysis of H_2O and CO_2. Journal of Power Sources. 2012;202:209-16.

[44] Zhan Z, Kobsiriphat W, Wilson JR, Pillai M, Kim I, Barnett SA. Syngas production by coelectrolysis of CO_2/H_2O: The basis for a renewable energy cycle. Energy & Fuels. 2009;23:3089-96.

[45] O'Brien JE, McKellar MG, Harvego EA, Stoots CM. High-temperature electrolysis for large-scale hydrogen and syngas production from nuclear energy – summary of system simulation and economic analyses. International Journal of Hydrogen Energy. 2010;35:4808-19.

[46] O'Brien JE, McKellar JG, Hawkes GL, Stoots CM. Development and validation of a one-dimensional co-electrolysis model for use in large-scale process modeling analysis. Fifth International Fuel Cell Science, Engineering, and Technology Conference. Brooklyn, N.Y.2007.

[47] Chen X, Guan C, Xiao G, Du X, Wang J-Q. Syngas production by high temperature steam/CO_2 coelectrolysis using solid oxide electrolysis cells. Faraday Discussions. 2015.

[48] Krey V, Masera O, Blanford G, Bruckner T, Cooke R, Fisher-Vanden K, et al. Annex II: Metrics & Methodology. In: Edenhofer O, Pichs-Madruga R, Sokona Y, Farahani E, Kadner S, Seyboth K, et al., editors. Climate Change 2014: Mitigation of Climate Change Contribution of Working Group III to the Fifth Assessment Report of the Intergovernmental Panel on Climate Change2014.

[49] von der Assen N, Jung J, Bardow A. Life-cycle assessment of carbon dioxide capture and utilization: avoiding the pitfalls. Energy & Environmental Science. 2013;6:2721-34.

List of tables

Table 1. Operating conditions of the carbon capture unit.

Parameter	Unit	Value
Absorber pressure	bar	1.2
Feed stream temperature to absorber	K	313
Regeneration column pressure	bar	1.9
Condenser temperature in regeneration column	K	317
Number of stages of absorber	-	10
Number of stages of stripper	-	6
MEA loading	-	0.35
MEA circulation rate	kmol h^{-1}	145400
MEA concentration	-	0.25
CO_2 removal efficiency	-	0.95
Flue gas rate	kmol h^{-1}	19000 for the hydrogenation 17580 for the HT SOEC

Table 2. Characteristics of the reactor and catalyst for the methanol synthesis.

Parameter	Unit	Value
Reactor length	m	7
Reactor tube diameter	m	0.04
Number of tubes	-	1620
Catalyst particle shape	-	Cylinder
Catalyst diameter	mm	5.4
Catalyst particle height	mm	5.2
Catalyst particle density	kg m^{-3}	1190
Void fraction of bed	-	0.285
Heat transfer coefficient	J $s^{-1}K^{-1}m^{-2}$	118.44

Table 3. Parameters for the kinetic model.

Index	A	B / J mol^{-1}
1	1.07	38500
2	3453.38	-
3	0.499	17197
4	6.62×10^{-11}	124119
5	1.22×10^{10}	-97900

Table 4. Parameter input for the modelling of the SOEC system

Parameter	Unit	Value	Source
i	A cm^{-2}	0.25	[45]
A_{cell}	cm^2	225	[45]
ASR^0	Ω cm^2	0.25	[45]

List of figures

Figure 7 HEN diagram for SOEC-based methanol production generated by Aspen AEA: (a) the integrated scenario, (b) carbon capture in the segregated scenario, (c) high-temperature electrolysis in the segregated scenario and (d) methanol synthesis in the segregated scenario.

Figure 8 Energy requirements for heating, cooling and electricity under the integrated and segregated scenarios in the methanol production by (a) CO_2 hydrogenation and (b) high-temperature CO_2 electrolysis. Comparison of total energy requirements of the two different CO_2-to-methanol processes when (c) the steam is used for electricity generation and (d) the steam is used as a heating medium. (e) Comparison of energy efficiencies of different CO_2-to-methanol process. A thermal-to-electricity efficiency of 60% is assumed when calculating energies.

Figure 9 Comparison of global warming impacts of methanol production by the different eTL processes.

Fig. 1.

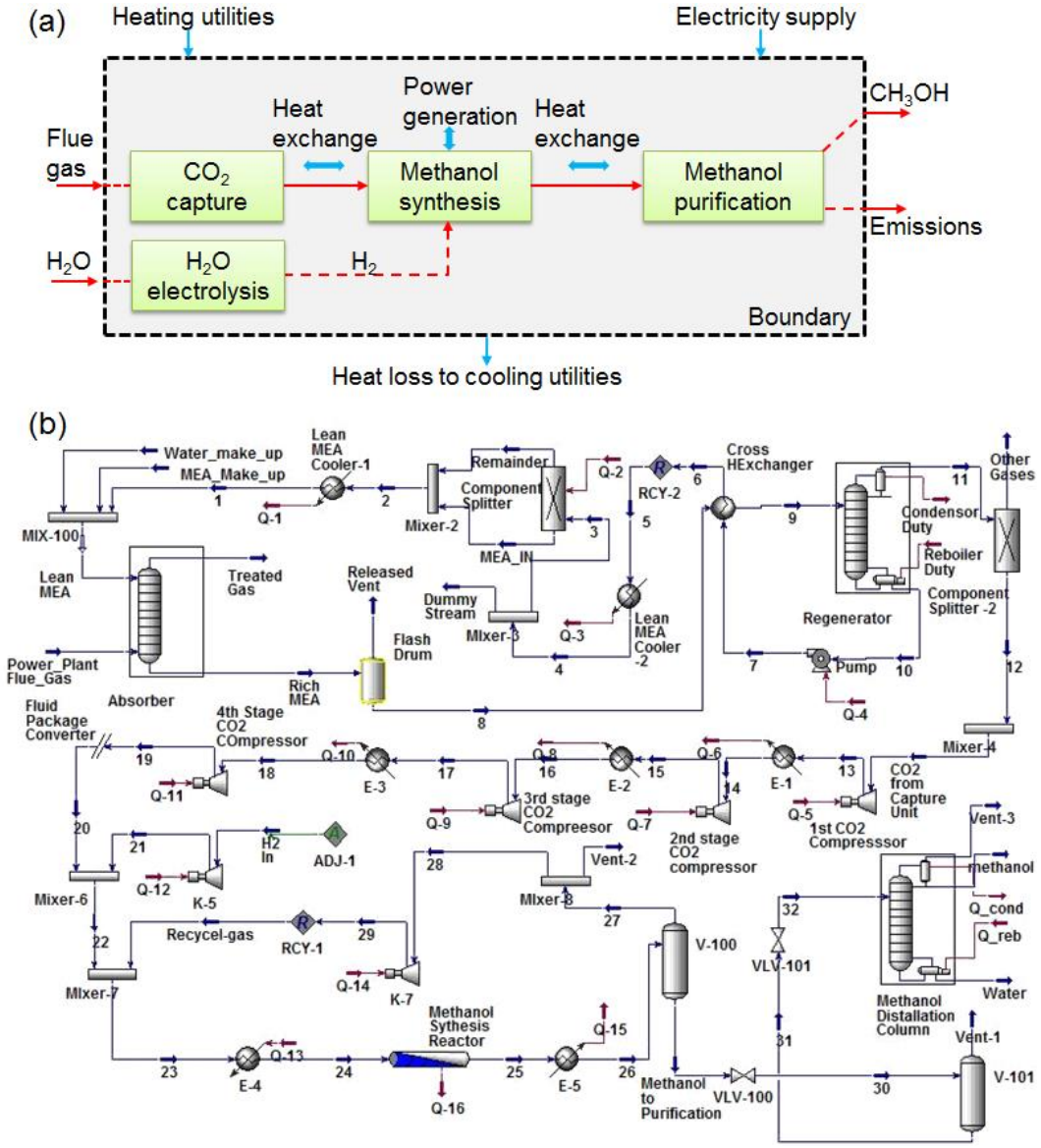
(a)
Heating utilities
Electricity supply
Power generation
Heat exchange
Heat exchange
Flue gas
CO_2 capture
Methanol synthesis
Methanol purification
CH_3OH
Emissions
H_2O
H_2O electrolysis
H_2
Boundary
Heat loss to cooling utilities
(b)
Water_make_up
MEA_Make_up
Lean MEA Cooler-1
Remainder
Component Splitter
Mixer-2
Q-2
RCY-2
Cross HExchanger
Other Gases
MIX-100
Q-1
MEA_IN
Condensor Duty
Reboiler Duty
Component Splitter -2
Lean MEA
Treated Gas
Released Vent
Dummy Stream
Mixer-3
Q-3
Lean MEA Cooler -2
Regenerator
Power_Plant Flue_Gas
Absorber
Flash Drum
Rich MEA
Pump
Q-4
Fluid Package Converter
4th Stage CO2 COmpressor
Q-10
E-3
Q-8
E-2
Q-6
E-1
Mixer-4
Q-11
3rd stage CO2 Compreesor
Q-9
Q-7
2nd stage CO2 compressor
Q-5
1st CO2 Compresssor
CO2 from Capture Unit
Vent-3
H2 In
ADJ-1
Vent-2
Mixer-6
Q-12
K-5
Mixer-8
methanol
Q_cond
Q_reb
Recycel-gas
RCY-1
V-100
VLV-101
Q-14
K-7
Methanol Sythesis Reactor
Methanol Distallation Column
Water
Mixer-7
Q-15
Vent-1
Q-13
E-4
E-5
V-101
Q-16
Methanol to Purification
VLV-100

Fig. 2.

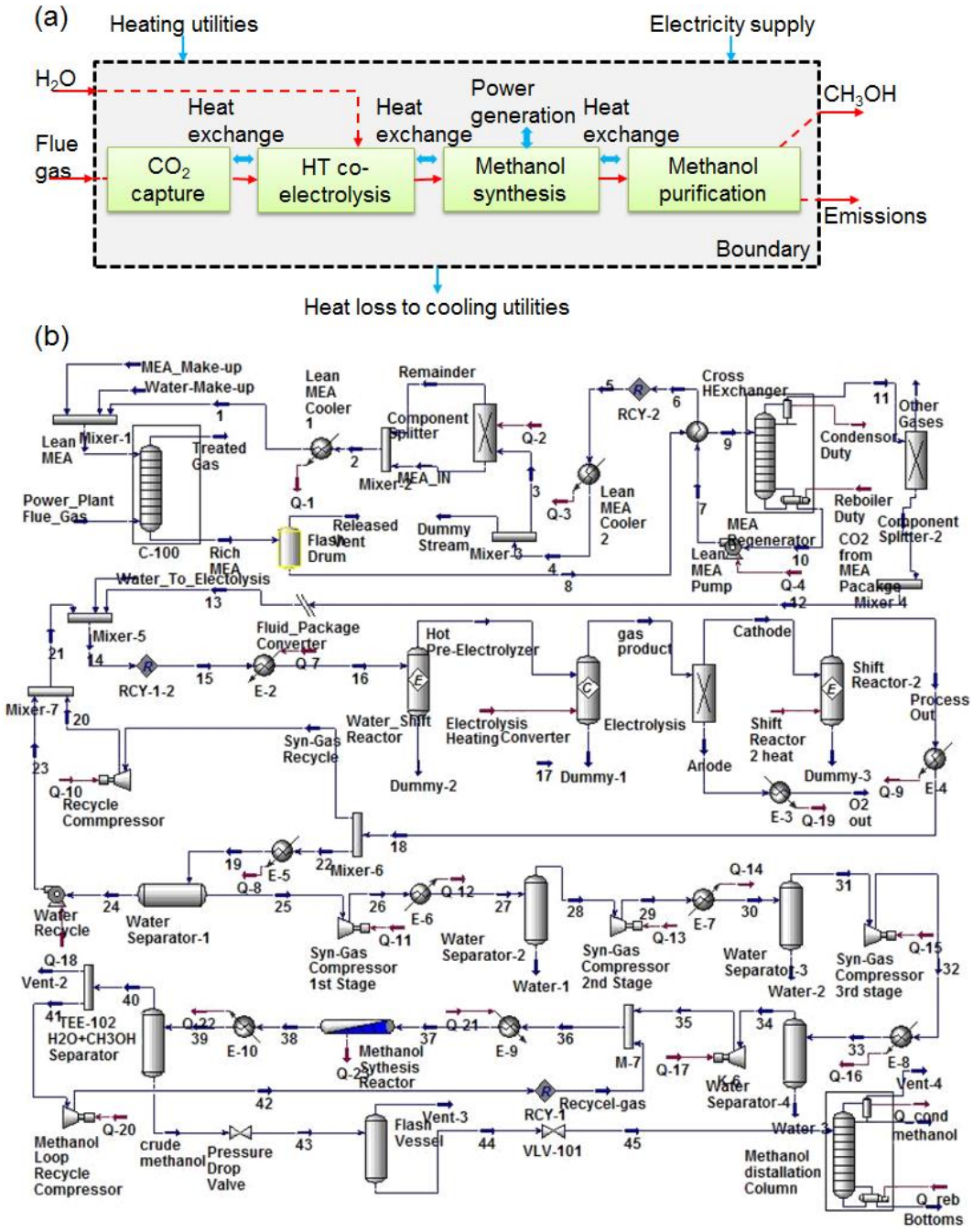
(a)
Heating utilities
Electricity supply
H_2O
Flue gas
Heat exchange
Heat exchange
Power generation
Heat exchange
CH_3OH
CO_2 capture
HT co-electrolysis
Methanol synthesis
Methanol purification
Emissions
Boundary
Heat loss to cooling utilities
(b)
MEA_Make-up
Water-Make-up
Lean MEA
Mixer-1
Treated Gas
Lean MEA Cooler 1
Component Splitter
Remainder
Q-2
MEA_IN
Mixer-2
Q-1
Power_Plant Flue_Gas
C-100
Rich MEA
Flash Drum
Released Vent
Dummy Stream
Mixer-3
Q-3
Lean MEA Cooler 2
RCY-2
Cross HExchanger
Condensor Duty
Other Gases
Reboiler Duty
MEA Regenerator
Lean MEA Pump
Q-4
CO2 from MEA Pacakge
Component Splitter-2
Mixer-4
Water_To_Electrolysis
Mixer-5
Fluid_Package Converter
Q-7
RCY-1-2
E-2
Hot Pre-Electrolyzer
gas product
Cathode
Shift Reactor-2
Process Out
Mixer-7
Water_Shift Reactor
Electrolysis Heating Converter
Electrolysis
Shift Reactor 2 heat
Syn-Gas Recycle
Dummy-2
Dummy-1
Anode
Dummy-3
Q-9
E-4
Q-10
Recycle Commpressor
E-3
Q-19
O2 out
Mixer-6
E-5
Q-8
Water Recycle
Water Separator-1
Q-12
E-6
Q-11
Syn-Gas Compressor 1st Stage
Water Separator-2
Water-1
Syn-Gas Compressor 2nd Stage
Q-13
E-7
Q-14
Water Separator-3
Water-2
Syn-Gas Compressor 3rd stage
Q-15
Q-18
Vent-2
TEE-102 H2O+CH3OH Separator
Q-22
E-10
Methanol Sythesis Reactor
Q-21
E-9
M-7
Q-17
K-6
Water Separator-4
E-8
Q-16
Vent-4
Recycel-gas
RCY-1
Q-20
Methanol Loop Recycle Compressor
crude methanol
Pressure Drop Valve
Flash Vessel
Vent-3
VLV-101
Water-3
Q_cond methanol
Methanol distallation Column
Q_reb
Bottoms

Fig. 3.

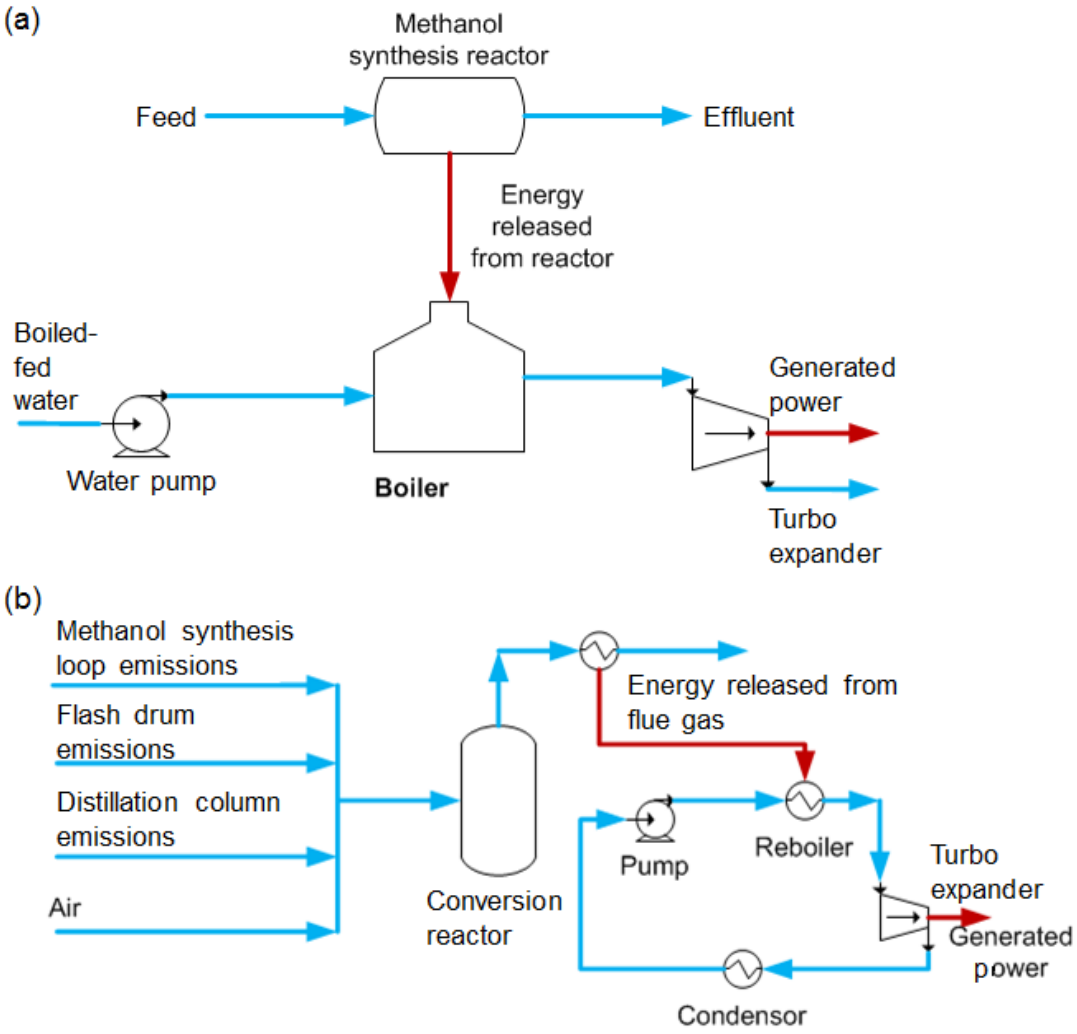
(a)
Methanol synthesis reactor
Feed
Effluent
Energy released from reactor
Boiled-fed water
Water pump
Boiler
Generated power
Turbo expander
(b)
Methanol synthesis loop emissions
Flash drum emissions
Distillation column emissions
Air
Conversion reactor
Energy released from flue gas
Pump
Reboiler
Turbo expander
Generated power
Condensor

Fig. 4

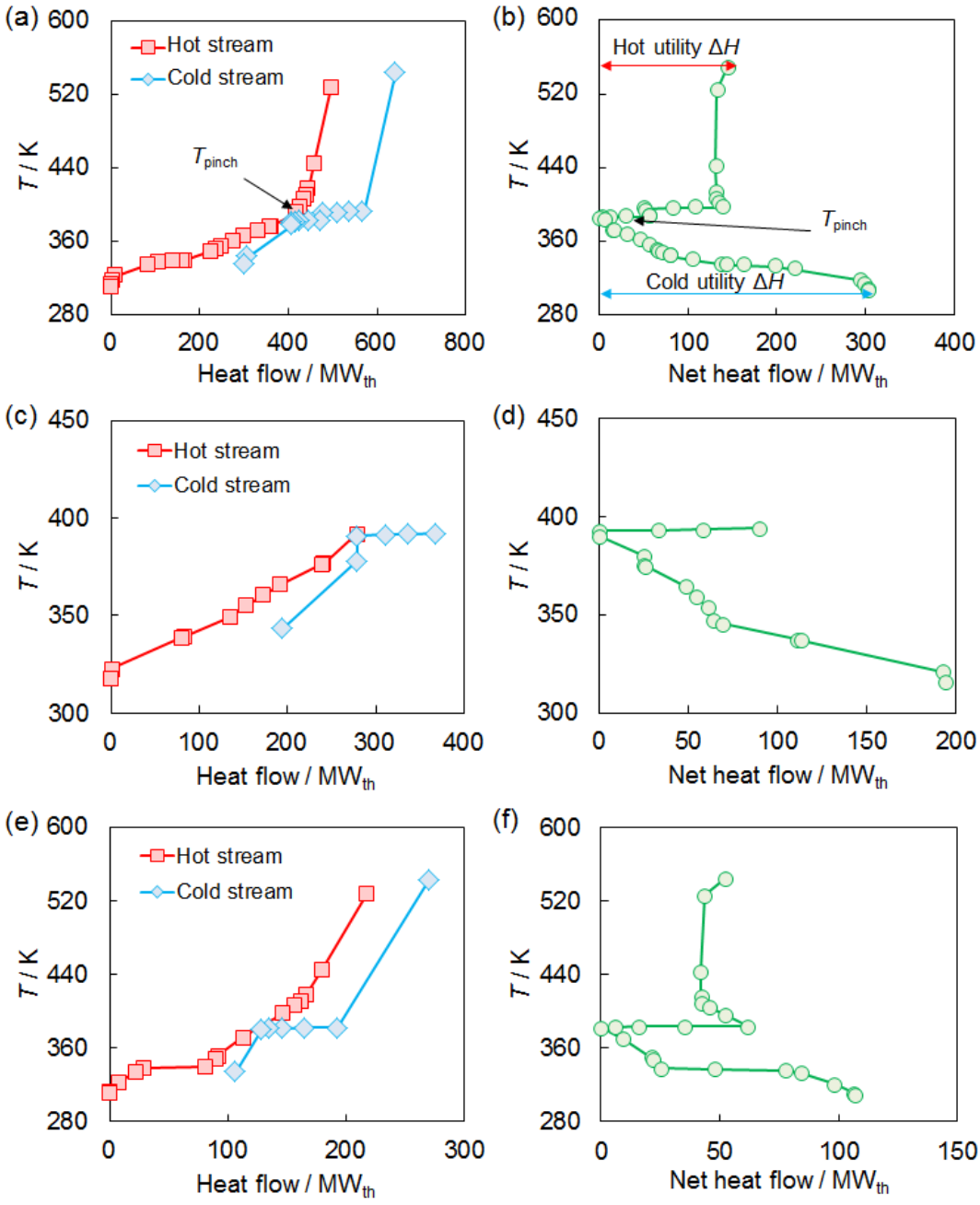
(a)
Hot stream
Cold stream
T_{pinch}
T / K
Heat flow / MW_{th}
(b)
Hot utility ΔH
T_{pinch}
Cold utility ΔH
T / K
Net heat flow / MW_{th}
(c)
Hot stream
Cold stream
T / K
Heat flow / MW_{th}
(d)
T / K
Net heat flow / MW_{th}
(e)
Hot stream
Cold stream
T / K
Heat flow / MW_{th}
(f)
T / K
Net heat flow / MW_{th}

Fig. 5

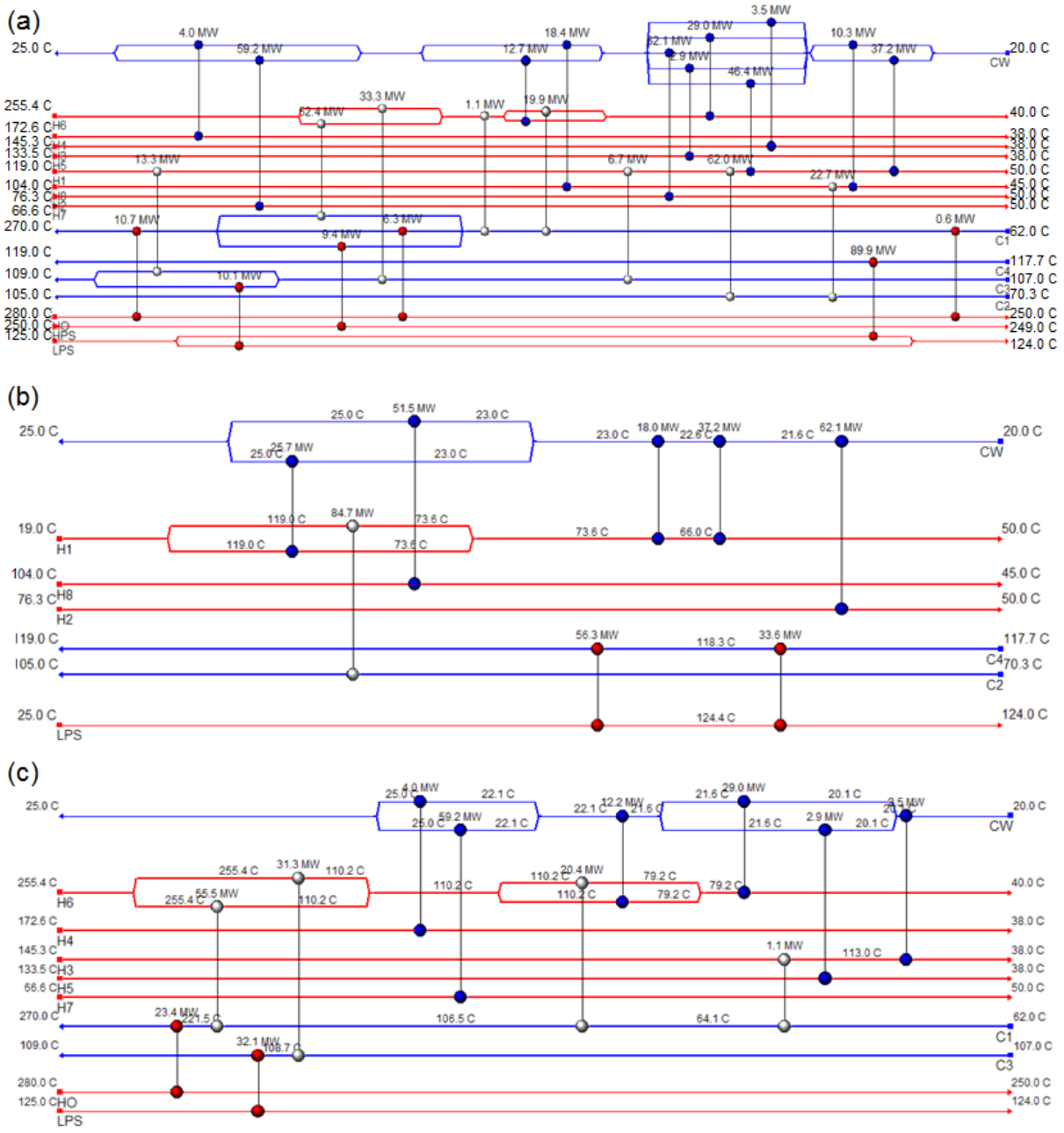
(a)
25.0 C
4.0 MW
59.2 MW
12.7 MW
18.4 MW
3.5 MW
29.0 MW
52.1 MW
2.9 MW
46.4 MW
10.3 MW
37.2 MW
20.0 C
CW
255.4 C
33.3 MW
52.4 MW
1.1 MW
19.9 MW
40.0 C
172.6 C
H6
38.0 C
145.3 C
H4
38.0 C
133.5 C
H3
38.0 C
119.0 C
H5
13.3 MW
6.7 MW
62.0 MW
22.7 MW
50.0 C
104.0 C
H1
45.0 C
76.3 C
H8
50.0 C
66.6 C
H7
50.0 C
270.0 C
10.7 MW
9.4 MW
6.3 MW
0.6 MW
62.0 C
C1
119.0 C
89.9 MW
117.7 C
109.0 C
10.1 MW
C4
107.0 C
105.0 C
C3
70.3 C
280.0 C
C2
250.0 C
250.0 C
H0
249.0 C
125.0 C
LPS
124.0 C
LPS
(b)
25.0 C
51.5 MW
25.0 C
23.0 C
25.0 C
25.7 MW
23.0 C
23.0 C
18.0 MW
22.6 C
37.2 MW
21.6 C
62.1 MW
20.0 C
CW
19.0 C
H1
119.0 C
84.7 MW
73.6 C
119.0 C
73.6 C
73.6 C
66.0 C
50.0 C
104.0 C
45.0 C
76.3 C
H8
50.0 C
H2
119.0 C
56.3 MW
118.3 C
33.6 MW
117.7 C
105.0 C
C4
70.3 C
C2
25.0 C
LPS
124.4 C
124.0 C
(c)
25.0 C
4.0 MW
25.0 C
22.1 C
59.2 MW
25.0 C
22.1 C
22.1 C
12.2 MW
21.6 C
21.6 C
29.0 MW
21.6 C
20.1 C
2.9 MW
20.1 C
3.5 MW
20.0 C
CW
255.4 C
31.3 MW
110.2 C
255.4 C
55.5 MW
255.4 C
110.2 C
110.2 C
110.2 C
20.4 MW
110.2 C
79.2 C
79.2 C
79.2 C
40.0 C
H6
172.6 C
38.0 C
H4
145.3 C
1.1 MW
113.0 C
38.0 C
133.5 C
H3
38.0 C
66.6 C
H5
50.0 C
H7
270.0 C
23.4 MW
221.5 C
106.5 C
64.1 C
62.0 C
C1
109.0 C
32.1 MW
108.7 C
107.0 C
C3
280.0 C
250.0 C
125.0 C
HO
124.0 C
LPS

Fig. 6

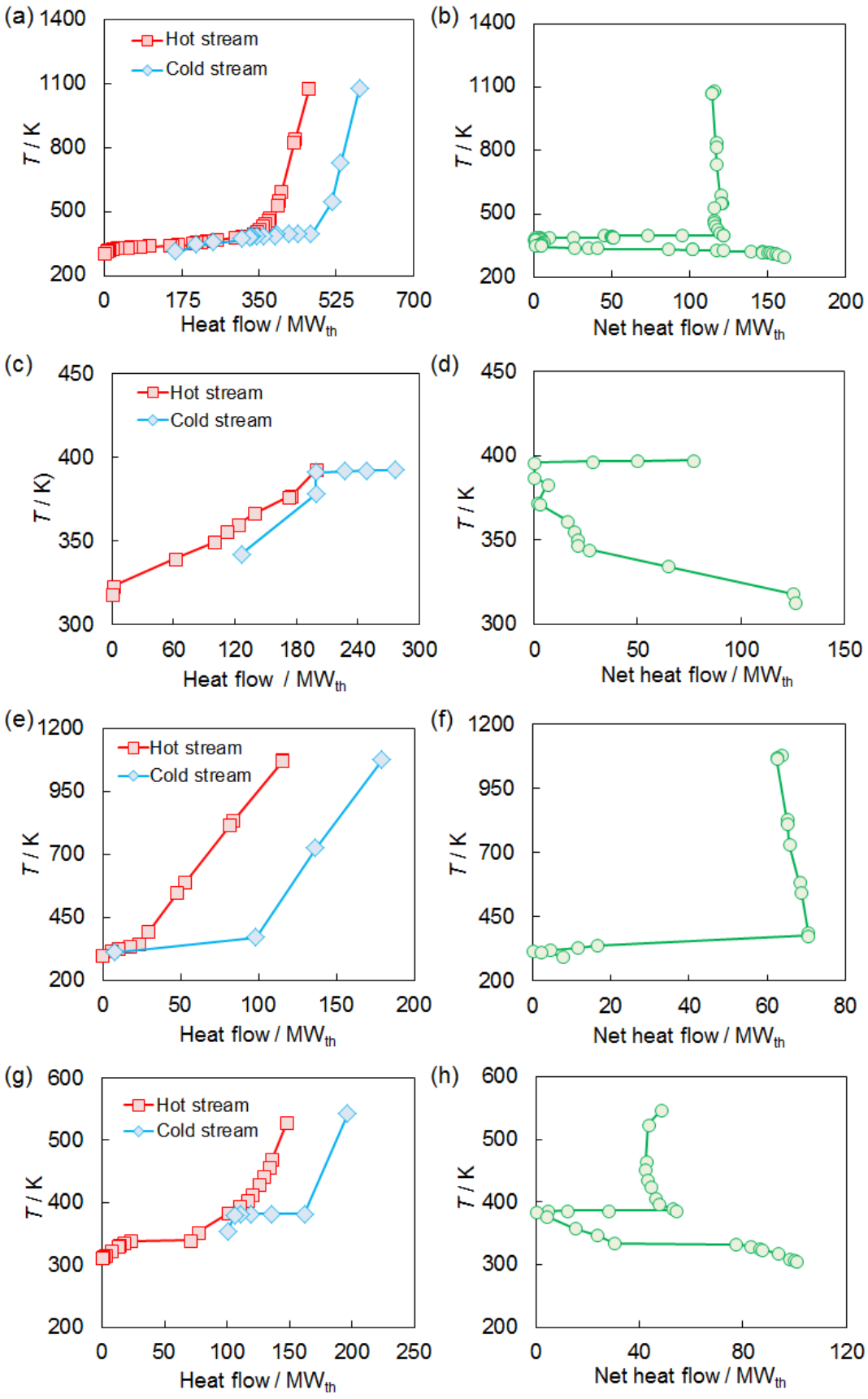
(a)
Hot stream
Cold stream
T / K
Heat flow / MWth
(b)
Net heat flow / MWth
(c)
T / K)
(d)
(e)
(f)
(g)
(h)

Fig. 7

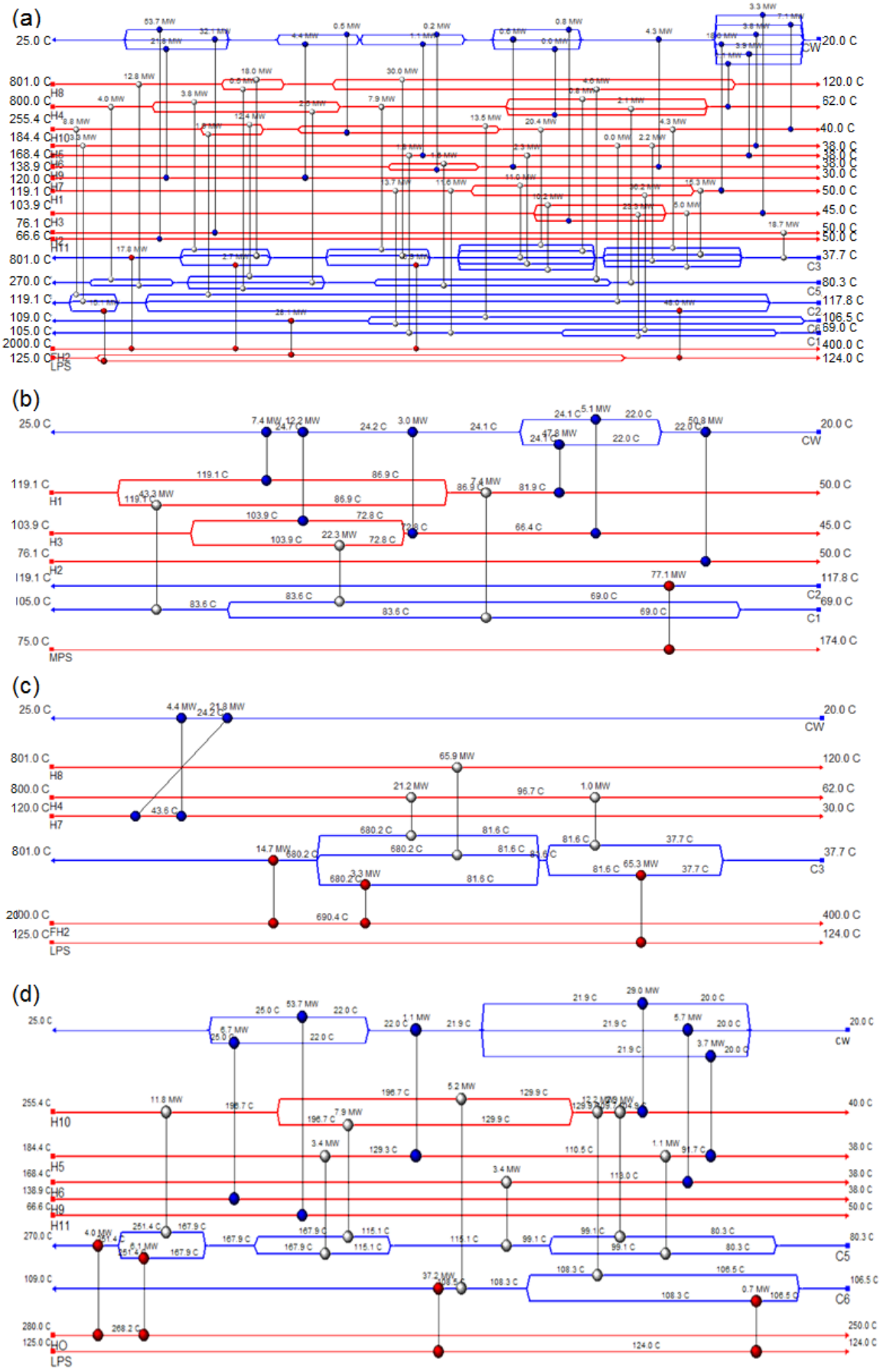
(a)
25.0 C
CW
20.0 C
801.0 C
H8
120.0 C
800.0 C
62.0 C
255.4 C
H4
184.4 C
H10
40.0 C
168.4 C
H5
38.0 C
138.9 C
H6
38.0 C
120.0 C
H9
30.0 C
119.1 C
H7
50.0 C
103.9 C
H1
45.0 C
76.1 C
H3
66.6 C
H12
50.0 C
801.0 C
H11
37.7 C
C3
270.0 C
80.3 C
C5
119.1 C
117.8 C
C2
109.0 C
106.5 C
C6
105.0 C
69.0 C
C1
2000.0 C
400.0 C
125.0 C
H2
LPS
124.0 C
(b)
25.0 C
CW
20.0 C
119.1 C
H1
50.0 C
103.9 C
H3
45.0 C
76.1 C
50.0 C
119.1 C
H2
117.8 C
105.0 C
C2
69.0 C
C1
75.0 C
MPS
174.0 C
(c)
25.0 C
CW
20.0 C
801.0 C
H8
120.0 C
800.0 C
62.0 C
120.0 C
H4
H7
30.0 C
801.0 C
37.7 C
C3
2000.0 C
400.0 C
125.0 C
FH2
LPS
124.0 C
(d)
25.0 C
CW
20.0 C
255.4 C
H10
40.0 C
184.4 C
38.0 C
168.4 C
H5
38.0 C
138.9 C
H6
38.0 C
66.6 C
H9
50.0 C
H11
270.0 C
80.3 C
C5
109.0 C
106.5 C
C6
280.0 C
250.0 C
125.0 C
HO
LPS
124.0 C

Fig. 8.

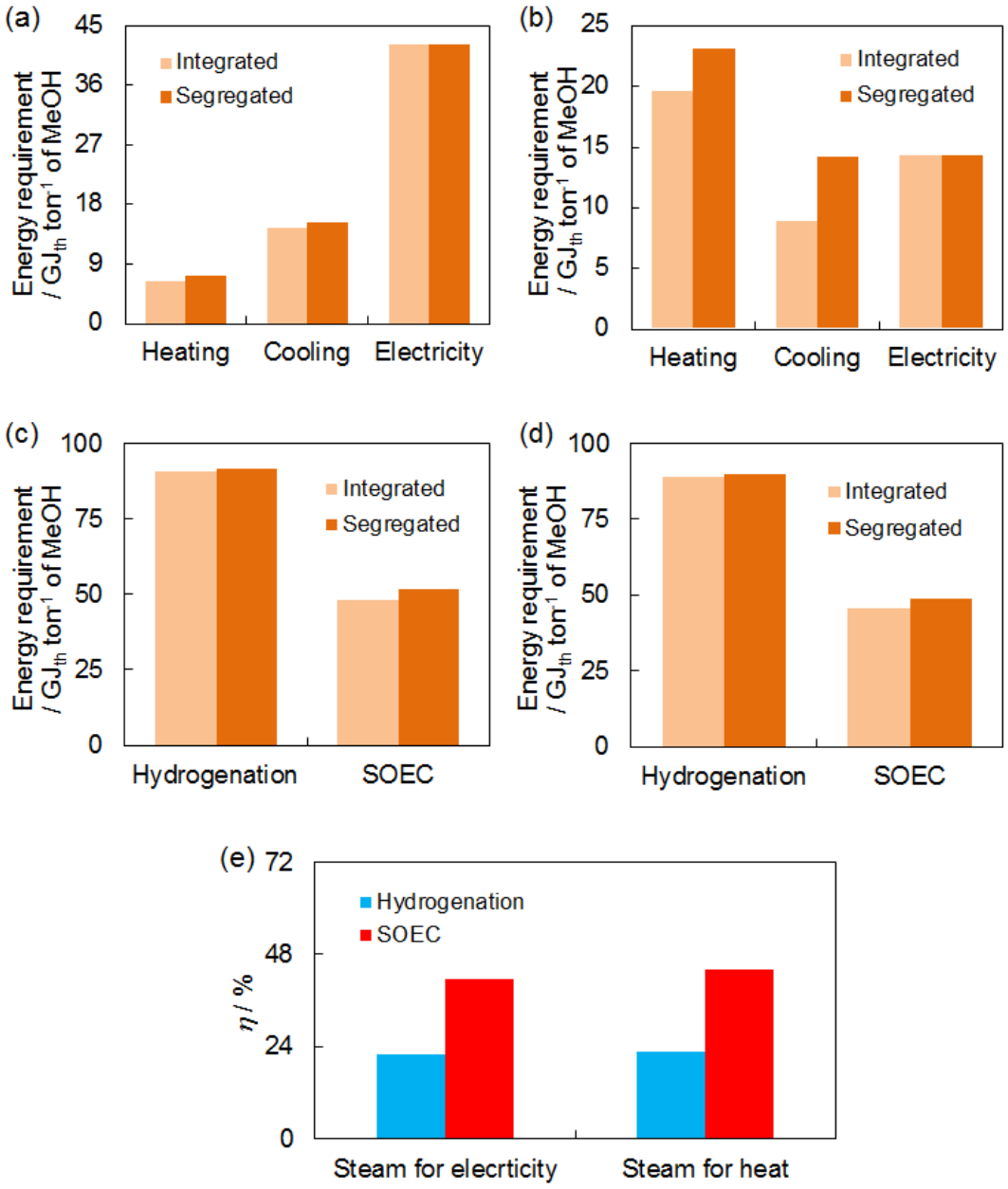
(a)
Energy requirement / GJth ton-1 of MeOH
45
36
27
18
9
0
Integrated
Segregated
Heating
Cooling
Electricity
(b)
Energy requirement / GJth ton-1 of MeOH
25
20
15
10
5
0
Integrated
Segregated
Heating
Cooling
Electricity
(c)
Energy requirement / GJth ton-1 of MeOH
100
75
50
25
0
Integrated
Segregated
Hydrogenation
SOEC
(d)
Energy requirement / GJth ton-1 of MeOH
100
75
50
25
0
Integrated
Segregated
Hydrogenation
SOEC
(e)
η / %
72
48
24
0
Hydrogenation
SOEC
Steam for elecrticity
Steam for heat

Fig. 9

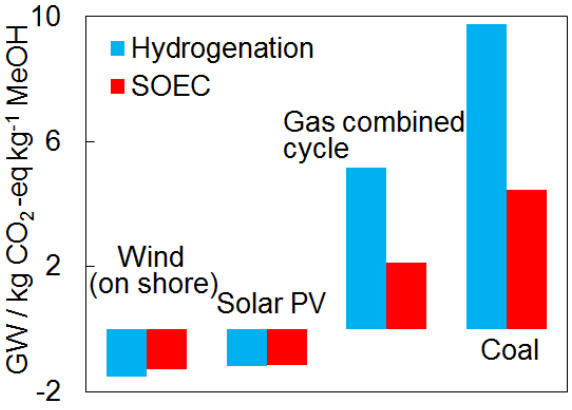
GW / kg CO_2-eq kg^{-1} MeOH
10
6
2
-2
Hydrogenation
SOEC
Gas combined cycle
Wind (on shore)
Solar PV
Coal